

The Optics of Semiconductor Diode Lasers

Masud Mansuripur and Ewan M. Wright

Robert N. Hall, born in New Haven, Connecticut in 1919, joined General Electric's Research and Development Center after graduating from the California Institute of Technology. In 1962, having realized that a semiconductor junction could support population inversion, Hall built the first semiconductor injection laser. This device, based on a specially designed p-n junction, operated when an electric current injected the electrons directly into the junction, thus allowing for highly efficient generation of coherent light from a compact source. Today, diode lasers based on Hall's original idea are used, among other places, in CD and DVD players, laser printers, and fiber-optic communication systems.¹

In this article we describe the basic features of the beam of light emitted by a diode laser, and discuss methods to analyze and manipulate this beam. Collimation and beam-shaping with a pair of cylindrical lenses will be shown to be a simple and flexible method that may be applied not only to diode lasers but also to beams emerging from optical fibers.

Characteristics of diode lasers

A semiconductor diode laser shown schematically in Fig. 1 consists of a gain layer (only a few ten nanometers thick), surrounded by guiding layers for confining the laser mode. The guiding layers' index of refraction is somewhat greater than that of the surrounding regions (substrate and cladding), thus permitting confinement by total internal reflection. The electrical current is injected through the positive electrode, a metallic stripe several microns wide, and collected at the base-plate on the opposite side of the junction (ground electrode). The population inversion and optical gain are strongest beneath the positive electrode, tapering off laterally with an increasing distance from the electrode's center line along Z . In gain-guided lasers, this tapering off of the gain is responsible for lateral beam confinement. (By contrast, in index-guided lasers the regions adjacent to the guiding stripe are selectively etched away, then replaced by a lower-index cladding material.) In general, the gain layer is highly absorptive in regions that are not directly underneath the electrode and, therefore, experience weak pumping or no pumping at all. The guiding layers are essentially transparent, except for losses due to scattering at impurities and at the interfaces. The substrate and the cladding are also highly transparent.

Figure 2 shows plots of intensity and phase at the front facet of a single-transverse-mode diode laser ($\lambda_0 = 980$ nm). The assumed beam divergence angles (full-width-at-half-maximum intensity

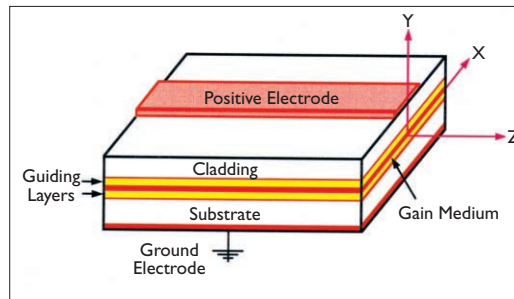


Figure 1. A semiconductor diode laser consisting of an active layer surrounded by guiding layers for confinement of the laser mode. The electrical current, injected through the positive electrode, is collected on the opposite side of the junction by the ground electrode.

or FWHM) are $\theta_{||} = 7^\circ$ in the plane of the junction and $\theta_{\perp} = 35^\circ$ perpendicular to the junction. In the top row of the figure, (a, b), where the assumed beam has no astigmatism, the phase distribution at the laser's front facet is uniform. In the middle row, (c, d), the astigmatic distance (defined as an equivalent distance in free space between horizontal and vertical beam waists) is $\Delta z = 10$ μm , resulting in a slightly wider beam along the X -axis, and a divergent phase front whose peak-to-valley variation (i.e., from the edge to the center of the beam) is $\sim 120^\circ$. In the bottom row, (e, f), the assumed astigmatism is $\Delta z = 25$ μm .

Again the beam is broader (in the horizontal direction) than the one without astigmatism, and the phase distribution exhibits a peak-to-valley variation of $\sim 190^\circ$.

The elliptical cross-section of the beam emerging at the front facet of the laser is responsible (through diffraction) for $\theta_{||}$ being much smaller than θ_{\perp} . The cause of astigmatism is the non-uniform gain profile (along the X -axis) within the active region of the laser. As the gain is strongest near the cavity's central axis, the beam, while propagating in the cavity along Z , experiences a "gain focusing" effect toward this axis—a direct consequence of stronger amplification on-axis than in the wings.² Consequently, a divergent phase profile automatically evolves for countering this tendency of the beam to collapse to the center. We will have more to say about this property in the following section.

Another interesting property of a diode laser beam is its polarization state, which is typically linear, having E -field parallel to the plane of the junction. This property may be traced back to the fact that, for light polarized parallel to the junction (i.e., $E_{||}$) the gain is somewhat greater than that for perpendicularly polarized light (hereinafter E_{\perp}). The guided mode associated with E_{\perp} is slightly broader in the Y -direction than the mode associated with $E_{||}$. Since a broad mode has less overlap with the gain layer than a more compact mode, it stays behind while the compact mode surpasses the threshold and begins to lase. Moreover, confinement of electrons and holes to a thin (quantum well) active layer makes it easier for $E_{||}$ (relative to E_{\perp}) to stimulate the excited electrons and holes into surrendering their photons and returning to the ground state. In practice a combination of both effects is responsible for promoting the selection of $E_{||}$ polarization over E_{\perp} .

Origin of diode laser astigmatism

The non-uniformity of the gain profile along X has a focusing effect on the guided mode that is countered automatically by a divergent phase front imposed on the beam as it propagates along the Z -axis of the cavity. An easy demonstration is provided by

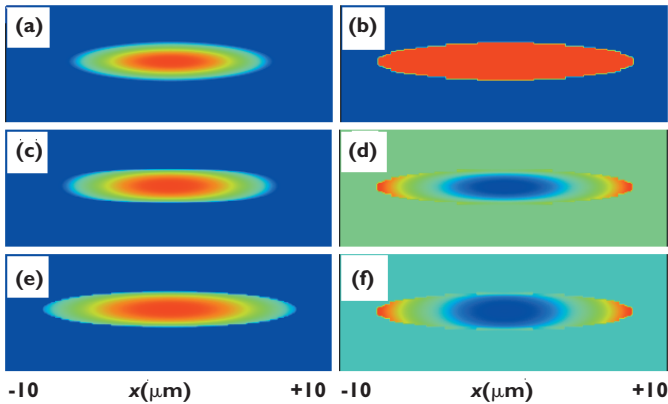


Figure 2. Plots of the logarithm of intensity (left) and phase (right) at the front facet of a $\lambda_o=980$ nm diode laser having $\theta_{||}=7^\circ$, $\theta_{\perp}=35^\circ$. The range of variations of intensity between the maximum (red) and minimum (blue) is $I_{\max}:I_{\min}=10^4$. In (a, b) the beam has no astigmatism. In (c, d) the astigmatic distance (in free space) between the horizontal and vertical beam waists is $\Delta z=10$ μm , resulting in a wider beam along X, and a divergent phase pattern whose variation from the center (blue) to the edge (red) is 120° . In (e, f), where the assumed astigmatism is $\Delta z=25$ μm , the beam is further broadened and the phase distribution exhibits a peak-to-valley variation of 190° .

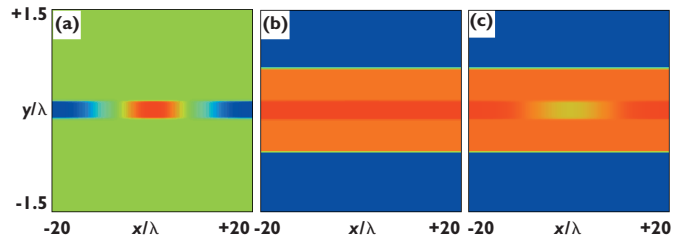


Figure 3. Profiles of two amplitude-phase masks used in BPM simulations of a diode laser beam. (a, b) represent the amplitude and phase profiles for Mask 1, (a, c) the corresponding profiles for Mask 2. The gain medium is a 0.25λ -thick layer sandwiched between two 0.5λ -thick guiding layers. (a) Transmitted intensity distribution for a uniform incident beam. The amplitude gain at the center is 1.025, tapering off along X to a (lossy) value of 0.95. Outside the active layer, the 0.995 amplitude transmissivity represents a weak background loss. (b) The phase of Mask 1 is 6.12° within the active layer, 5.4° in the guiding layers, and 0° in the substrate and cladding. (c) The phase of Mask 2 (having the same amplitude profile as in (a)) is 4.5° at the center of the active layer; 6.12° within the active layer far from the axis, 5.4° in the guiding layers, and 0° in the substrate and cladding.

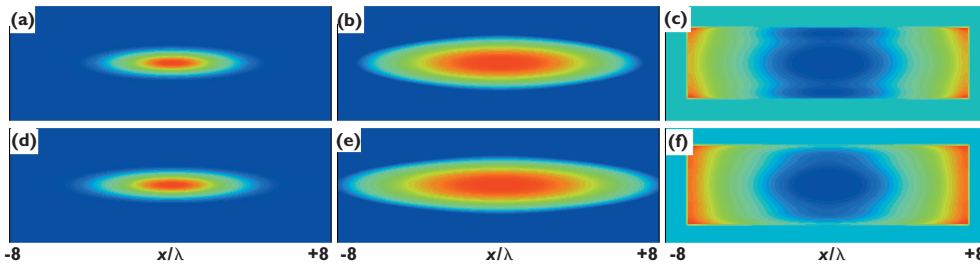
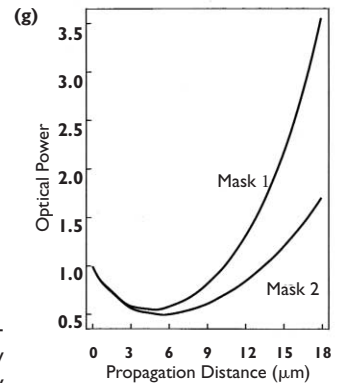


Figure 4. Plots of (a) intensity, (b) logarithm of intensity, and (c) phase after 600 BPM steps. The amplitude-phase Mask 1 used in these simulations is depicted in Figs. 3(a, b). The light is seen to be confined to the guiding layers, with a weak evanescent tail leaking into the substrate and cladding. In (c) the peak-to-valley phase variation along X is 160° . The bottom row (d-f) is similar to the top row (a-c), except that it is obtained with Mask 2 depicted in Figs. 3(a, c). In (f) the peak-to-valley phase variation along X is 175° . (g) Power content of the beam versus propagation distance in the BPM simulations.



studying the propagation of a beam of light through a gain medium using the Beam Propagation Method (BPM).³ Figure 3(a) shows the distribution of gain (red) and loss (blue) in the cross-sectional plane of a typical diode laser. The gain is significant only in the middle section of the gain layer, dropping off in a Gaussian fashion along the X-axis and becoming a loss in the regions remote from the central axis, Z. During propagation along the cavity's Z-axis, the phase profile imparted to the beam's cross-section is similar to that shown in Fig. 3(b). Here the high-index guiding layers (orange) advance the phase relative to the lower-index substrate and cladding (blue). The gain medium (red) with its slightly higher index advances the phase even more than the guiding layers do, but the gain layer is thin, and its contribution to mode confinement along the Y-axis is fairly insignificant.

Together, the cross-sectional intensity and phase distributions shown in Figs. 3(a, b) define the profile of an amplitude-phase mask that can be used in a BPM simulation of a diode laser. This particular mask is placed at intervals of $\Delta z = 0.1\lambda$ between propagation steps in a medium of refractive index $n_o = 3.3$. (The wavelength λ in this environment is λ_o/n_o , where λ_o is the free-

space wavelength of the laser beam.) For a uniform beam incident on the mask, the transmitted intensity and phase distributions appear in Figs. 3(a, b), respectively. The assumed gain medium is a 0.25λ -thick layer sandwiched between two 0.5λ -thick layers of slightly lower refractive index, which constitute the guiding slab. The amplitude gain at the center of the active layer is 1.025 (per 0.1λ of propagation), tapering off in a Gaussian fashion along the X-axis while remaining uniform in the Y-direction. The background loss of the medium outside the active layer is small (mask amplitude transmission = 0.995), but within the gain layer and far from the central axis, the light amplitude is attenuated by a factor of 0.95 (per 0.1λ of propagation). In Fig. 3(b), the phase of the mask is 6.12° within the active layer, 5.4° in the two adjacent (guiding) layers, and 0° in the substrate and cladding regions. This means, for example, that if the index of the substrate and cladding materials is $n_o = 3.3$, then the guiding layers have index $n_1 = 3.45$ and the active medium has index $n_2 = 3.47$.

In practice, pumping the gain medium causes a decline in its local index, so that a more realistic phase mask would be similar to that shown in Fig. 3(c), where the phase at the center of the ac-

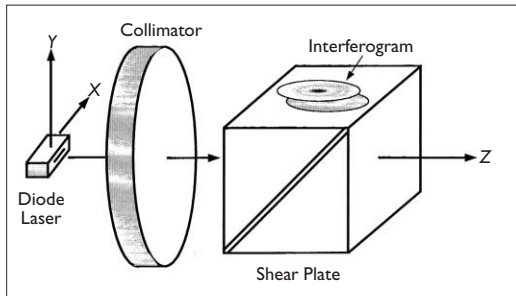


Figure 5. A single-transverse-mode beam from a diode laser is captured and collimated by an aberration-free lens, then analyzed with a shear-plate interferometer. Any phase variations in the cross-section of the beam show up as fringes in the shearing interferogram.

tive region has dropped to 4.5° (corresponding to $n_2 = 3.425$). From this minimum, the phase increases in a Gaussian fashion along the X -axis, reaching the value of 6.12° in the highly absorptive regions of the active layer. This results in index anti-guiding along the X -axis (due to index inhomogeneity within the active layer). The Gaussian phase profile inside the active layer imposes on the laser beam a divergence (along X) above and beyond that imposed by the gain profile alone.^{4,5} The rest of the mask is identical to that in Fig. 3(b). In what follows, we will first show results of BPM simulations obtained with the amplitude-phase Mask 1, depicted in Figs. 3(a, b), confirming that the gain profile alone can give rise to astigmatism. We then show results of simulations obtained with the amplitude-phase Mask 2, shown in Figs. 3(a, c), which reveal that the index “anti-guiding” of the gain medium (caused by population inversion) can further enhance the induced astigmatism.

Figure 4, top row, shows plots of (a) intensity, (b) logarithm of intensity, and (c) phase after 600 steps of BPM using Mask 1. Since each step corresponds to a propagation distance of 0.1λ inside a medium of refractive index $n_0 = 3.3$, the total propagation distance in this simulation is $\sim 18 \mu\text{m}$. The light is seen to be well-confined to the guiding layers, with only a small fraction leaking (i.e., evanescent) into the substrate and cladding. The light that escapes the guiding layers is eventually lost by scattering or diffraction out of the system. In Fig. 4(c), the peak-to-valley phase variation along X is 160° , corresponding to a divergent beam with a few microns of astigmatism. The bottom row in Fig. 4 is similar to the top row, except that it is obtained with Mask 2. The beam is somewhat broader along the X -axis when compared to that obtained without an index anti-guiding of the gain medium. Also, the peak-to-valley phase variation in Fig. 4(f) is 175° (along X), corresponding to a divergent beam with somewhat more astigmatism than the one depicted in Fig. 4(c).

Figure 4(g) shows plots of the power content of the beam versus propagation distance z , as obtained in the above simulations. At first, the power decreases as the initial beam adjusts itself to the guiding structure, shedding excess light that does not match the guided mode profile. The gain medium then takes over and raises the power content exponentially, as the confined mode propagates along the optical axis.

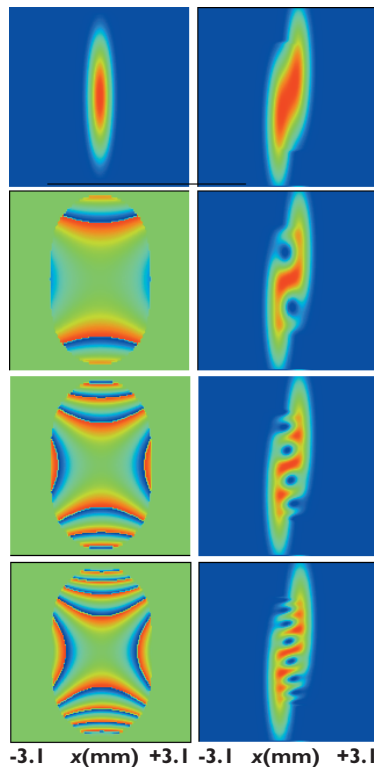


Figure 6. Left column: Plots of intensity (top) and phase in a plane located 10 mm beyond the exit pupil of the collimator of Fig. 5. The 0.6NA lens is one focal length ($f = 4.9 \text{ mm}$) away from the mid-point between the two waists of the laser beam ($\lambda_0 = 980 \text{ nm}$, $\theta_{||} = 7^\circ$, $\theta_{\perp} = 35^\circ$). Right column: Intensity patterns at the viewing window of the shear plate ($\Delta x = 0.7 \text{ mm}$, $\Delta y = 2.0 \text{ mm}$). From top to bottom, the assumed astigmatism of the laser is 0, 10, 20, 30 μm .

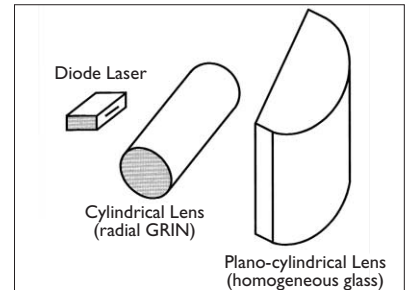


Figure 7. Collimation of a diode laser beam by a pair of cylindrical lenses. The first lens collimates the beam along the fast axis, while the second lens arrests the expansion of the beam along the slow axis.

Shearing interferometry

The beam of a single-transverse-mode diode laser may be captured and collimated by an aberration-free lens, then analyzed using a shear-plate interferometer, as shown in Fig. 5. The shear plate creates two identical copies of the collimated beam shifted relative to each other along the X - and/or Y -axes. Superposition of these two copies of the same beam at the observation plane creates an interferogram that reveals the phase structure of the (collimated) beam. Any phase non-uniformities at the exit pupil of the collimator show up as intensity variations (i.e., fringes) in the interferogram.

For a $7^\circ \times 35^\circ$ beam emerging from a $\lambda_0 = 980 \text{ nm}$ diode laser, Fig. 6 (left column) shows plots of intensity (top) and phase in a plane located 10 mm past the exit pupil of a 0.6NA collimator lens. The lens is at a distance of $f = 4.9 \text{ mm}$ from the mid-point between the two waists of the laser beam and the displayed phase patterns correspond to $\Delta z = 10, 20, 30 \mu\text{m}$ of astigmatism. For a fixed shear of $\Delta x = 0.7 \text{ mm}$ (horizontal) and $\Delta y = 2.0 \text{ mm}$ (vertical), the right column in Fig. 6 shows the observed interference patterns in the viewing window of the shear plate; from top to bottom, the assumed astigmatism of the laser is $\Delta z = 0, 10, 20, 30 \mu\text{m}$.

Beam collimation using a cylindrical lens pair

A diode laser’s beam may be collimated by a pair of cylindrical lenses, as shown in Fig. 7. In this scheme the first lens has the responsibility of collimating the beam along its fast divergence axis, while the second lens arrests the expansion of the beam along its slow axis. When a divergence angle is large, a gradient index (GRIN) cylindrical lens provides more collimation power as well as better correction for residual aberrations.

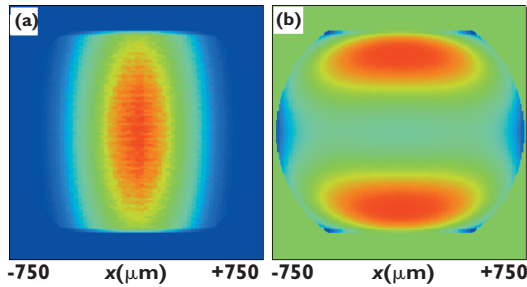


Figure 8. Plots of (a) intensity, (b) phase of a laser beam ($\lambda_0=980$ nm, $\theta_{||}=7^\circ$, $\theta_{\perp}=35^\circ$, astigmatism $\Delta z=0$) upon emerging from the lens pair of Fig. 7. For the particular lenses chosen in this simulation, the optical power throughput is $\sim 80\%$, the r.m.s. wavefront aberration is 0.19λ , and the peak-to-valley phase variation across the aperture is $\sim 280^\circ$.

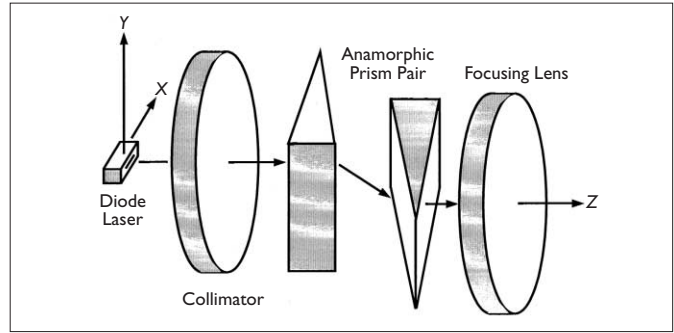


Figure 9. A diode laser's beam is collimated, then shaped by a prism pair that expands the beam's diameter along the X-axis. The collimated and anamorphically magnified beam is subsequently focused by an aberration-free lens identical to the one used for collimation.

As a concrete example, consider a single-transverse-mode beam having $\lambda_0=980$ nm, $\theta_{||}=7^\circ$, $\theta_{\perp}=35^\circ$, and astigmatism $\Delta z=0$. The first lens is a 5 mm-long cylindrical rod of radius $r_0=1.5$ mm, made of GRIN material having $n(r)=1.59 [1-0.04455(r/r_0)^2]$; the clear aperture diameters of the lens are $\Delta x=5.0$ mm, $\Delta y=1.2$ mm. The distance between the front facet of the laser and the first surface of this lens is 0.348 mm. The second lens, a plano-cylinder made of homogeneous glass of index $n=1.65$, is separated by 0.397 mm from the first lens; its thickness (along the optical axis) is 3.2 mm, is 5 mm long, has a 3 mm radius of curvature, and its clear aperture diameter is 1.5 mm. All lens surfaces are anti-reflection coated.

Figure 8 shows computed plots of intensity and phase at an observation plane located 0.3 mm beyond the plano-cylindrical lens of Fig. 7. The fraction of the optical power captured by the lens pair is nearly 0.8, and the r.m.s. wavefront aberration at the observation plane is $\sim 0.19\lambda_0$. The same lens pair (with a slight adjustment of the separation between its two elements) may be used for collimation in the presence of astigmatism on the laser beam, without any degradation of the wavefront quality.

By allowing the slow axis of the beam to propagate further before being collimated, the cylindrical lens pair enables one to adjust the degree of ellipticity of the beam's cross-section. Of course, the requisite physical parameters of the second lens depend on the desired minor-to-major-axis ratio of the collimated beam, but, in principle, any degree of ellipticity can be achieved. Thus, the cylindrical lens pair not only collimates the divergent beam of a diode laser, but it also allows shaping (in particular, circularization) of the beam's cross-section.

Anamorphic magnification and beam compression

Figure 9 shows an aberration-free lens collimating a diode laser's beam, followed by a pair of anamorphic prisms that expand the beam along the X-axis. This collimated and anamorphically magnified beam is subsequently focused by an aberration-free lens identical with the one used initially for beam collimation. Because the laser beam's divergence angles parallel and perpendicular to the plane of the junction are widely different (i.e., $\theta_{||} \ll \theta_{\perp}$), the collimated beam's diameter along X is typically much less than that along Y. Expanding the beam along X until it fills the entrance pupil of the focusing lens, enables one to obtain a focused spot substantially smaller (in one dimension) than the bright spot appearing at the front facet of the laser.

Figure 10 shows computed plots of intensity and phase at several cross-sections of the system of Fig. 9. The assumed parameters of the laser are $\lambda_0=980$ nm, $\theta_{||}=7^\circ$, $\theta_{\perp}=35^\circ$, astigmatism $\Delta z=0$. Both the collimator and the focusing lens have $NA=0.6$, $f=4.9$ mm, and the prism pair's magnification factor $M=5.5$ (along X) is sufficient to circularize the beam's cross-section. The top row in Fig. 10 shows the beam at the front facet of the laser. The second row shows that before entering the prisms the beam has an elliptical cross-section with an aspect ratio of ~ 5.5 . Emerging from the prism pair (third row) the beam is circularized. The bottom row shows the focused spot at the focal plane of the focusing lens; this compressed image of the bright elliptical spot at the front facet of the laser has circular symmetry and a much reduced diameter along the X-axis.

Figure 11 is similar to Fig. 10, except for the position of the diode laser along the X-axis, which is shifted to $x=-20$ μm . Collimation and anamorphic magnification work as before, but the beam emerging from the collimator is tilted by about 0.23° away from the Z-axis. The prism pair magnifies the beam along X by ~ 5.5 , but it also reduces the tilt of the beam by the same factor. The net result is that the image of the bright elliptical spot at the front facet of the laser, in addition to being compressed in size, is brought closer to the optical axis at $x=+3.6$ μm . This is an important result which may be applied, for instance, to compressing incoherent laser beams. A typical high-power, multi-transverse-mode diode laser may have the same divergence angles as above (i.e., $7^\circ \times 35^\circ$), but its bright area at the front facet is much larger, say, $\sim 1 \times 50$ μm^2 . The radiation profile of such lasers may be considered (approximately) to consist of a number of mutually incoherent filaments, each similar to the beam of a coherent (i.e., single-transverse-mode) diode laser. If, therefore, the central filament of an incoherent laser is identified with the coherent beam depicted in Fig. 10, then the marginal filament will be represented by Fig. 11. The system of Fig. 9 can thus collimate the incoherent laser's various filaments (simultaneously and independently of each other), perform anamorphic magnification on each and every one of them, then create (at the focal plane of the last lens) a string of closely packed focused spots along the X-axis. In doing so the system of Fig. 9 creates a compressed image of the elongated bright spot at the front facet of the incoherent laser. (In the present example the image size will be $\sim 1 \times 10$ μm^2 .) The achievable compression is roughly equal to the ratio $\theta_{\perp}/\theta_{||}$ of the divergence angles.

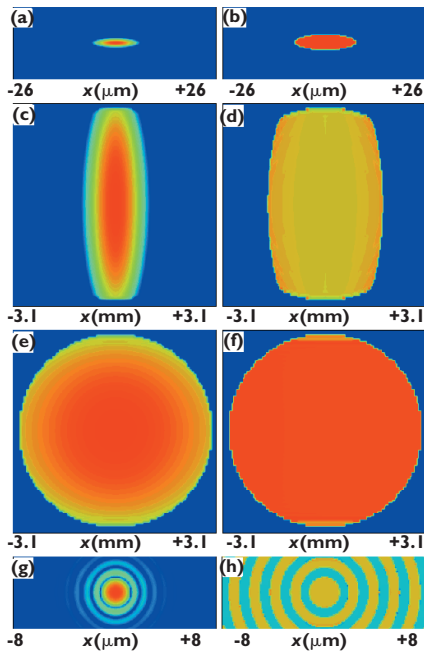


Figure 10. Distributions of the logarithm of intensity (left) and phase (right) at several cross-sections of the system of Fig. 9. The lenses have NA=0.6, $f=4.9$ mm. The prisms are made of $n=1.72$ glass, and have an apex angle of 69° . (a, b) Front facet of the laser. (c, d) Exit pupil of the collimator, just before entering the prism pair. (e, f) Emerging from the second prism. (g, h) Focal plane of the focusing lens.

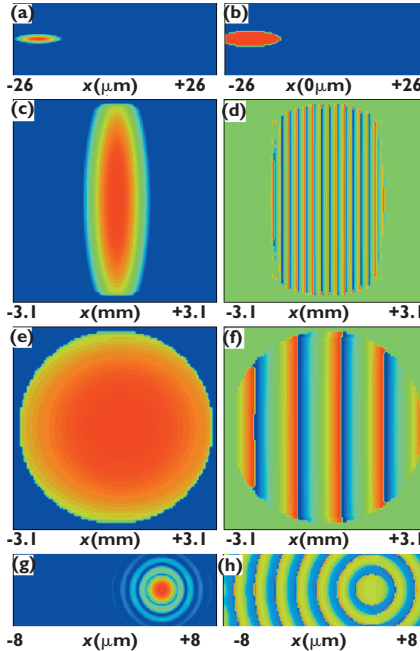


Figure 11. Same as Fig. 10 but with the diode laser shifted $20 \mu\text{m}$ to the left along the X-axis.

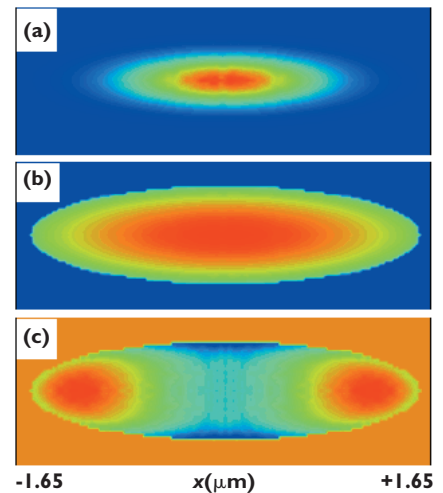


Figure 12. Plots of (a) intensity, (b) logarithm of intensity, (c) phase at the exit pupil of a cylindrical lens pair used as collimator and anamorphic magnifier for the beam emerging from a single-mode fiber ($\lambda_0 = 1.544 \mu\text{m}$). A $0.775 \times 3.1 \text{ mm}^2$ elliptical aperture is placed at the exit pupil to clip the edges of the beam. The overall transmission of the system is 95.5%, and the ratio of the FWHM beam diameters is 4.1. The peak-to-valley phase variation in (c) is 56° .

Cylindrical lenses for collimation and beam-shaping in fiber optics systems

A pair of cylindrical lenses (similar to those shown in Fig. 7) can be used in similar fashion to capture the beam emerging from an optical fiber. For example, a pair of GRIN cylinders can collimate and anamorphically magnify the beam emerging from a single-mode silica glass fiber. Unlike the beam from a diode laser, the emergent beam of a fiber is usually unpolarized, making cylindrical lenses superior to prism pairs in applications that demand anamorphic magnification with a low level of polarization-dependent loss.

Consider a cylindrical and a plano-cylindrical lens oriented at right angles to each other, as in Fig. 7. The GRIN profile of both lenses is $n(r) = 1.59[1 - 0.04455(r/r_0)^2]$, r being the radial distance from the cylinder axis, and r_0 the cylinder radius. The $1/e$ (amplitude) diameter of the single-mode Gaussian beam emerging from the fiber is $10 \mu\text{m}$ ($\lambda_0 = 1.544 \mu\text{m}$). The distance from the fiber facet to the first lens is 0.501 mm, radius of the first lens is 2 mm, separation between the lenses is 3.525 mm, and radius of the second lens is 6.7 mm, with its center of curvature located on the plane facet of the lens. The cylinder lengths should be large enough to accommodate the beam, but are otherwise arbitrary. All surfaces are anti-reflection coated.

Figure 12 shows computed plots of intensity, logarithm of intensity, and phase at the exit pupil of the lens pair. The first lens arrests the spread of the beam in the vertical-direction, while the beam continues to spread in the horizontal direction (and become elongated) until its capture by the second lens. The overall trans-

mission of the system is 95.5%, and the ratio of FWHM beam diameters at the exit pupil is 4.1. (The anamorphic magnification factor can be further increased if the first lens is made proportionately smaller or the second lens larger). The phase plot shows a small amount of astigmatism, with a peak-to-valley variation of $\sim 56^\circ$ (r.m.s. wavefront aberrations=0.035). The aberrations may be reduced if the plano-cylindrical lens is replaced by a full cylinder. Alternatively, a different index profile of the GRIN rods or a smaller aperture stop could help reduce these aberrations.

When used in conjunction with a one-dimensional array of fibers, one of the lenses can be shared among the various fibers. Similarly, in a 2-D square array of fibers, the fibers in each row can share the first lens, while the fibers in each column can share the second lens. Collimation of a 10×10 fiber array will thus require only 10 cylinders of each type.

Acknowledgment

The authors are grateful to Mahmoud Fallahi of the Optical Sciences Center for helpful discussions.

References

1. Adapted from <web.mit.edu/invent/www/inventors>.
2. L.V. Casperson and A.Yariv, "Gain and dispersion focusing in a high gain laser," *Applied Optics* **11**, 462-466 (1972).
3. M. Mansuripur, E. M.Wright, and M. Fallahi, "The Beam Propagation Method," *Optics & Photonics News* **11** (7), 42 (2000).
4. F.R. Nash, "Mode guidance parallel to the junction plane of double-heterostructure GaAs lasers," *J.Appl. Phys.* **44**, 4696-4707 (1973).
5. D. D. Cook and F.R. Nash, "Gain-induced guiding and astigmatic output beam of GaAs lasers," *J.Appl. Phys.* **46**, 1660-1672 (1975).

OPN contributing editor Masud Mansuripur <masud@u.arizona.edu> is a professor of Optical Sciences at the University of Arizona in Tucson. His collection of past OPN columns has recently been published in *Classical Optics and Its Applications* (Cambridge University Press, UK, 2002). Ewan Wright is a professor of Optical Sciences at the University of Arizona.